Energy &
Environment Nexus

Original Research

Open Access

https://doi.org/10.48130/een-0025-0003

Unveiling an overlooked pathway of water arsenic contamination: microscale evidence of enhanced arsenic mobility from the rhizosphere to detritusphere of macrophytes

Cai Li[1], Xin Ma[2], Xue Jiang[1,3], Youzi Gong[1], Xiaolong Wang[1], Musong Chen[1], Qin Sun[4*] and Shiming Ding[5*]

Received: 10 June 2025

Revised: 6 July 2025

Accepted: 28 July 2025

Published online: 16 October 2025

Abstract

The global decline of submerged macrophytes is accelerating, yet the processes involved in arsenic (As) mobilization in sediments remain poorly understood, particularly during the transition from the rhizosphere to the detritusphere. This study monitored the spatio-temporal variations of As, Iron (Fe), and associated microbial communities during root growth and degradation processes of macrophytes using high-resolution sampling and high-throughput sequencing techniques. Results showed that the As-depletion zones in the rhizosphere transformed into release hotspots of As after the death of macrophytes, resulting in an upward flux of 12.43 ng/cm^2/d from sediments. This shift was driven by the significant changes in redox conditions and microbial functions related to Fe and As transformation. Transitioning from the aerobic rhizosphere to the anaerobic detritusphere, the relative abundance of Fe(III)-reducing bacteria increased by 81.23%, contributing to approximately 90% of Fe-bound As lost from Fe plaque. Furthermore, the significant decline in As(III) oxidase genes and methylation genes may have inhibited the oxidation and methylation of As(III), subsequently enhancing the availability and mobility of As in sediments. Thus, this transition fundamentally alters the fate of sediment from sinks to sources of As, highlighting unanticipated threats to water quality in light of widespread loss of macrophytes.

Keywords: Arsenic, Submerged macrophyte, Sediment, Iron plaque, Microbial community

Highlights

- High-resolution sampling and analysis methods were used to study As mobilization.
- Fe plaque sequestration and microbial transformations reduced As bioavailability.
- Macrophyte loss transformed sediment from As sink into release hotspots.
- Reductive dissolution of Fe-oxides and bioreduction enhanced As bioavailability.

* Correspondence: Qin Sun (sunqinnj@hhu.edu.cn); Shiming Ding (smding@seu.edu.cn)
Full list of author information is available at the end of the article.

Graphical abstract

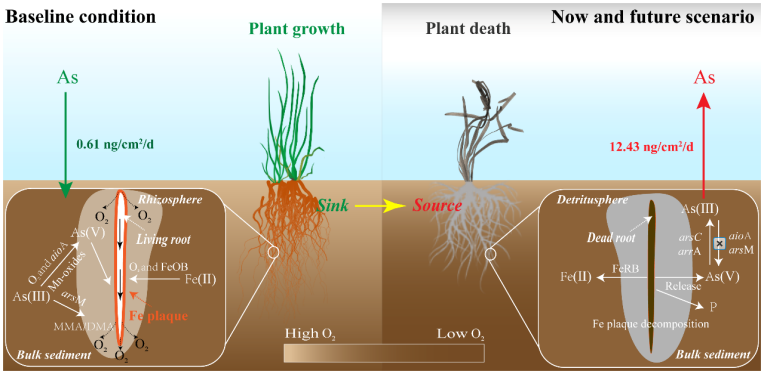

Introduction

Arsenic (As) has attracted widespread attention because of its serious adverse effects on humans, such as skin cancers[1]. Among the various exposure pathways, contamination of water by As is probably the greatest threat, as it poses a significant health risk to human populations through either direct ingestion or indirect food chain pathways[2]. Arsenic enters the surface water by both natural processes, such as oxidative/reductive dissolution of As-bearing minerals, and anthropogenic activities, such as discharge of As-containing wastewater, and eventually accumulates in sediments, resulting in much higher As concentrations than the baseline in sediments[3]. The concern is that As can be released back into the overlying water from sediments in response to changes within the aquatic environment, such as elevated temperatures or reduced oxygen (O_2) levels[4,5]. The primary mechanism for the release of As from sediments is widely acknowledged to be the reductive dissolution of As-bearing iron (Fe) or manganese (Mn) oxides[6]. Research has shown that the release flux of soluble As across the sediment interface can reach up to 130.2 ng/cm^2/d under hypoxic bottom-water environments, directly elevating its concentration in the overlying water from <10 μg/L to approximately 70 μg/L[7]. Consequently, understanding the potential factors enhancing the As mobilization in sediments is essential for mitigating As contamination risks of water bodies.

Macrophytes, especially submerged species, constitute a vital component of aquatic ecosystems, and their root activities can affect As mobilization in sediments[8]. Macrophytes generally release O_2 from their roots into the anoxic sediments, which is referred to as radial O_2 loss (ROL)[9]. This process not only directly oxidizes Fe(II) to Fe(III), but also enhances the activity of Fe(II)-oxidizing microbes[10]. Both processes drive the development of Fe plaques on root surfaces, consisting primarily of poorly crystalline Fe minerals including ferrihydrite and lepidocrocite[11], which immobilize As via adsorption and co-precipitation reactions[12]. The ROL-driven As(III) oxidation processes in the rhizosphere, including the chemical oxidation by Mn-oxides[13] and the biological oxidation by those microbes with As(III) oxidase genes (*aio*A)[9,14], can reduce As mobility and bioavailability, as the oxidation products As(V) can be further sequestered by root Fe plaques.

There has been a substantial decline in submerged macrophytes over the last 40 years, due to human activities and climate change[15,16]. After the death of macrophytes, however, the sediment characteristics are reshaped around the decaying roots[17], which may reverse the rhizosphere sequester mechanism from an accumulation zone to a release hotspot, and thereby become a source of aqueous As contamination. Decaying roots cannot release O_2, meaning the subsequent cessation of ROL causes a shift in condition from an aerobic rhizosphere to an anaerobic detritusphere[18]. The reductive dissolution of low crystalline Fe-oxides in the Fe plaque under O_2 limitation may be enhanced[19], potentially resulting in the rapid release of As into the porewater[20]. Furthermore, the transition from the rhizosphere to the detritusphere initiates a succession of microbial communities, from those that utilize root exudates for energy to those that specialize in decomposing more refractory organic litter[21]. These changes in microbes could significantly alter As biotransformation processes, thereby influencing its speciation and mobility. For example, As(V)-reducing microbes encoding respiratory As(V) reductase genes (*arr*A) could reduce As(V) to gain energy under anaerobic conditions[14], further increasing the As mobility. Despite the high risk of As release during the apoptosis of macrophytes, the transformations of Fe and As, and their implications for As mobilization are not well understood, particularly in the context of the global decline in macrophytes[22].

Our limited understanding of As mobilization and transformation in the rhizosphere stems from its steep gradient of chemical, physical, and biological profiles along the millimeter to sub-millimeter scale, especially considering its temporal dynamics[23]. Until recently, research progress has been facilitated by advanced microscale sampling techniques, coupled with a variety of spectroscopic and microscopic techniques[24,25]. Herein, we combined some novel research approaches to unravel the mobilization and transformation processes of As in sediments before and after macrophyte death. Our objectives were to: (i) monitor the spatiotemporal dynamics of As and related parameters by using planar optodes (PO), high-resolution dialysis (HR-Peeper), and the diffusive gradients in thin films (DGT); (ii) investigate the effects of Fe-mineral transformations on As mobility by combining Mössbauer spectroscopy and chemical extraction schemes; and (iii) explore how the structural and functional characteristics of microbiota change and affect As mobilization through high-throughput sequencing and real-time quantitative polymerase chain reaction (qPCR), from rhizosphere to detritusphere. The findings are crucial for understanding the potential future threats to sediment As release and associated water contamination risks.

Materials and methods

Microcosm experiment

Vallisneria natans was chosen as a case study owing to its widespread distribution in global aquatic ecosystems and common application in

the field of ecological restoration[26]. *V. natans*, surface sediments, and water samples were collected from Lake Taihu, China, in June 2022. *V. natans* was one of the dominant macrophytes in Lake Taihu; however, the area where they grow has been sharply decreased since the 1990s due to water pollution and eutrophication[27]. The basic characteristics of the water and sediment are presented in Supplementary Tables S1 and S2. Sediments were passed through a mesh (150 μm) to eliminate large particles and benthic infauna, and water was filtered through a filter membrane (0.45 μm). Sediments were subsequently placed into 12 Perspex tubes (diameter 11 cm, length 35 cm) and six transparent rhizoboxes equipped with detachable windows (height 25 cm, length 10 cm, width 5 cm).

Two microcosm experiments were set up to study the mobilization processes of As during the transition from the rhizosphere to the detritusphere (Supplementary Fig. S1). In the first microcosm experiment, four Perspex tubes were used as a group to monitor the dynamics in redox conditions and soluble As levels in sediments with root growth and subsequent root degradation. In the second microcosm experiment, two rhizoboxes were used as a group to visualize the two-dimensional (2D) distribution of O_2 and labile As within both the rhizosphere and detritusphere. For both first and second microcosm experiments, triplicate experiments were performed. To ensure consistency in the experimental material, young *V. natans* with an aboveground length of approximately 10 cm were selected for incubation. Their roots were cut to retain only about 1 cm in length before transplantation.

For the first microcosm experiment, Perspex tubes were incubated in a water tank maintained at 25 °C. The light conditions consisted of an intensity of 180 μmol photons/m^2/s, with a light:dark photoperiod of 12:12 h. Two young *V. natans* were transplanted into the one Perspex tube and allowed to grow for 45 d to obtain a dense root system. Following this growth period, the aboveground parts were cut off to simulate plant wither[18], and further incubated for at least 15 d until roots showed significant degradation. In total, four sampling times were set up, each using three Plexiglas tubes. For the second microcosm experiment, rhizoboxes were incubated in a water tank at 25 °C (Supplementary Fig. S1). The temperature and light conditions were consistent with those used in the first experiments. Two young *V. natans* were transplanted into transparent rhizoboxes and positioned at a 45° angle to ensure that the roots developed along the detachable side[18]. To avoid interference from DGT sampling on the rhizosphere environment, the same rhizoboxes were not chosen to compare the differences between the rhizosphere and detritusphere. Plants were first allowed to grow for 20 d, and then the aboveground parts were cut off and further cultivated for at least 15 d until roots showed significant degradation. Rhizoboxes have a smaller volume compared to Perspex tubes, and therefore the growth period of *V. natans* was adjusted to 20 d to avoid the dense root systems.

Microelectrode and HR-Peeper measurement

In the first microcosm experiment, the vertical profiles of dissolved O_2 (DO) and redox potential (Eh) in sediments were determined at unplanted stage (0 d), growth stage I (15 d), growth stage II (45 d), and decomposition stage (> 60 d) by using a microelectrode system (Unisense, Denmark), with the probe positioned near the plant to capture the impact of root growth and degradation on sediment redox conditions. Sediment porewater was sampled using HR-Peeper samplers (EasySensor Ltd., China). This sampler operates on the principle of diffusive equilibrium between sediment porewater and deionized water in the sampler chamber[28]. At different stages, HR-Peeper samplers were inserted into the sediment near the plant and left to equilibrate for 72 h. Soluble As, Fe, and UV254 in the porewater were subsequently analyzed with a spatial resolution of 5.0 mm. UV254 absorbance, a well-established proxy for aromatic dissolved organic matter (DOM)[29], was utilized to monitor root decomposition dynamics in this study (Supplementary Fig. S2).

PO and DGT measurement

In the second microcosm experiment, the PO and DGT techniques were employed for mapping O_2 and labile As in sediments. PO is often used for measuring the temporal and spatial distribution of solutes in sediments via luminescence imaging of sensor films that contain fluorophores[30]. In this study, O_2 optodes were attached to the detachable windows, and luminescence image acquisition was performed daily using PO2100 imaging systems (EasySensor Ltd., China) to monitor the dynamic changes in O_2 from rhizosphere to detritusphere. The PO2100 imaging system integrates two 405 nm light-emitting diodes (LEDs), a complementary metal-oxide-semiconductor camera, and an embedded controller for synchronized light source and image acquisition management. A 460 nm long-pass filter was installed on the camera lens to reduce the interference of light. All image capture procedures were completed within a darkroom environment.

DGT, an *in situ* passive sampling technique, can obtain the labile fractions of solutes, including free ions, the weakly-bound fractions that can be released from complexes and solids[31]. The combination of DGT and laser ablation inductively coupled plasma mass spectrometry (LA ICP-MS) enables the mapping of 2D distributions of various solutes in sediments[32]. HR-ZCA DGT was utilized to visualize the distribution of labile As, Fe, Mn, P, and S(-II)[33]. Following O_2 imaging, the detachable windows equipped with O_2 optodes were replaced with HR-ZCA binding gels immobilized with polyvinylidene fluoride membranes and sealing tape, and deployed for 24 h.

After retrieval, DGT gels were vacuum-dried at 50 °C for 3 h. The quantitative analysis of multiple elements using LA ICP-MS was performed according to previously established methodology[33]. Laser ablation of dry DGT gel was performed using Resolution LR/S155 LA system equipped with Coherent Compex-Pro 193 nm ArF excimer laser, with aerosolized samples transported through He gas to the Agilent 7700 × ICP-MS to obtain the signal intensities of the target solute. The scanning speed, laser spot size, acquisition time, repetition rate, and energy output of the LA system were 50 μm/s, 100 μm, 0.006 s, 10 Hz, and 2.5 J/cm^2, respectively. As the major elemental component of the matrix of the binding gel, signals for ^{13}C as an internal normalization standard were recorded simultaneously[34]. The spatial resolution of both PO and DGT is 100 μm. The detailed fabrication procedures and processes of the PO and DGT are provided in the Supplementary File 1.

Sample collection and analysis

After DGT sampling, root Fe plaques, rhizosphere and detritusphere samples, as well as corresponding bulk sediment, were collected from the rhizoboxes in the second microcosm experiment. To minimize the impact of spatial heterogeneity, the same samples from each rhizobox were thoroughly mixed to form a composite sample. All samples were subjected to freeze-drying and kept at −80 °C until analysis. Each composite sample was analyzed in triplicate. Sediment genomic DNA was extracted using an OMEGA Soil DNA Kit (M5635-02) and subsequently subjected to 16S rRNA gene sequencing. The 515F/907R primer sets (5′-GTGCCAGCMGCCGCGGTAA-3′ and 5′-CCGTCAATTCMTTTRAGTTT-3′) were employed to sequence a specific segment of the prokaryotic 16S rRNA (V4–V5 hypervariable regions). Additionally, genes related to As transformation, including As(III) methylation (*ars*M),

As(III) oxidation (*aio*A), as well as As(V) reduction (*arr*A and *ars*C), were evaluated using qPCR[14]. Details regarding the primer pairs for As-cycling genes are summarized in Supplementary Table S3. 16S rRNA gene sequencing and qPCR measurement were performed on the Illlumina NovaSeq platform and LightCycler480II at Shanghai Personal Biotechnology Co., Ltd, China. Detailed sequencing procedures are given in the Supplementary File 1.

Iron mineral transformations from rhizosphere to detritusphere were studied using ^{57}Fe Mössbauer spectroscopy and chemical extraction. ^{57}Fe Mössbauer spectra were recorded at room temperature (295 K) using a proportional counter and Mössbauer Spectrometer (MFD-500AV-02), at the Center for Advanced Mössbauer Spectroscopy, Dalian Institute of Chemical Physics, Chinese Academy of Sciences (Dalian, China). Fe-oxides and other Fe-bearing mineral phases were identified according to their Mössbauer parameters, including isomer shift, quadrupole splitting, and magnetic hyperfine field[35]. A refined extraction method was used to determine Fe speciation, including acid volatile sulfide and carbonate-associated Fe(II), easily reducible Fe oxides, reducible Fe oxides, magnetite, and pyrite–Fe (Supplementary Table S4)[36]. Arsenic speciation was determined using the Shiowatana sequential extraction procedure, including water-soluble As (F_{S1}), surface-adsorbed As (F_{S2}), Fe/Al associated As (F_{S3}), acid-extractable As (F_{S4}), and residual As (F_{S5}) (Supplementary Table S5)[37]. Total Fe and As were extracted by a HNO_3–HF mixture. Fe and As concentrations in the extraction were measured using ICP-MS and ICP-atomic emission spectrometry (ICP-AES), respectively. Recoveries of Fe and As in the certified reference samples ranged from 93% to 108%.

Data analysis

The release flux of soluble As across the sediment interface (J, ng/cm^2/d) was calculated utilizing data obtained from HR-Peepers in accordance with Fick's First Law[38]:

$$J = -\varphi D_S \left(\frac{\partial C}{\partial X}\right)_{X=0} \quad (1)$$

where, φ is the sediment porosity, D_s is the diffusion coefficients of As in sediments, and $(\frac{\partial C}{\partial X})_{X=0}$ refers to the concentration gradient over a distance of 20 mm below the sediment interface.

For O_2 fluorescence images, the red and green channels were extracted to calculate the O_2 concentration. The concentration gradient of O_2 around roots was used to calculate the ROL per area of root surface (ROL rate)[39]. A thin diffusion layer of 0.10 mm thickness is utilized in the measurement of DGT. Thereby, its results are generally interpreted as representing the time-averaged flux of the analyte (pg/cm^2/s)[40]. Detailed data analysis of PO and DGT is provided in the Supplementary File 1.

Amplicon sequences were quality-controlled and analyzed via the QIIME (Quantitative Insights Into Microbial Ecology) platform, version 2. The composition, structure and alpha (α) diversity of microbial communities were assessed using the 'vegan' package in R. The differentially abundant taxa across groups were identified using the linear discriminant analysis effect size (LEfSe) through the 'microeco' package in R. The Functional Annotation of Prokaryotic Taxa (FAPROTAX) tool was used to evaluate Fe metabolic functions. Sequence data from this study have been uploaded to the NCBI Sequence Reads Archive (PRJNA1047963).

Correlation analysis was conducted using the Spearman method. Significant differences were assessed using the Mann–Whitney U-test. Statistical analyses were conducted using SPSS 27.0 software.

Results

Changes in redox conditions from the rhizosphere to the detritusphere

As shown in Fig. 1a, b, the O_2 penetration depths were −12.5 and −18.5 mm at the growth stage I and II of *V. natans*, respectively, which were 3.5 mm and 9.5 mm deeper compared to the unplanted stage. At the root decomposition stage, the O_2 penetration depth decreased to −6 mm. The Eh in sediments also exhibited similar changes. Average Eh values in sediments increased from 211.48 to 279.60 mV with the root growth, and decreased to 167.81 mV after the death of plants. Root growth of macrophytes can improve the Eh in sediments, while degradation of macrophyte roots decreases it.

ROL occurred along all visible roots of *V. spiralis* according to O_2 imaging, causing the formation of an oxic area situated about 4–20 mm away from the center of the root (Fig. 2 and Supplementary Fig. S3). The O_2 concentration was highest in the zones of the root-dense part, and gradually decreased to the root tips. The ROL rate ranged from 2.10 to 35.13 nmol/m^2/s, which is comparable to previously reported values (Supplementary Table S6)[41]. After plant death, root O_2 release stopped, with the aerobic rhizosphere being transformed into an anaerobic detritusphere (Fig. 2 and Supplementary Fig. S3).

Changes in soluble As in sediments with root growth and degradation

The soluble As levels decreased in both the overlying water and porewater during growth of *V. spiralis* (Fig. 1c and Supplementary Fig. S4). In the overlying water, soluble As concentrations were 7.82 ± 0.34 and 1.40 ± 0.69 μg/L at growth stages I and II of *V. natans*, respectively, significantly lower than those at the other two stages ($p < 0.01$). In the porewater, the soluble As concentration during *V. natans* growth was approximately 3.5-fold lower than that during the period of no growth and withering. Furthermore, the release flux of soluble As decreased from 7.62 to −0.61 ng/cm^2/d with the *V. natans* growth, while it increased to 12.43 ng/cm^2/d after the death of *V. natans*.

Spatial distribution of labile As in the rhizosphere and detritusphere

High-resolution chemical imaging showed that the labile As fluxes in all visible rhizosphere were lower than those in the bulk sediments (Fig. 2 and Supplementary Fig. S5). Labile As flux was 17.63 ± 4.67 pg/cm^2/s in the rhizosphere, less than half that in the bulk sediment (35.88 ± 7.15 pg/cm^2/s) (Supplementary Figs S6 and S7). Reduction in labile As within approximately 5 mm of the rhizosphere was observed. After plant death, localized hotspots of labile As occurred, spatially more concentrated around the detritusphere. Labile As flux was 27.54 ± 3.97 pg/cm^2/s in the detritusphere, which was significantly greater than that in the bulk sediments (18.05 ± 2.56 pg/cm^2/s) ($p < 0.01$). There was a localized approximate twofold increase in labile As from rhizosphere to detritusphere. Additionally, labile fluxes of Fe, P, and S(-II) also increased from rhizosphere to detritusphere, whereas labile Mn showed the opposite trend (Fig. 2 and Supplementary Fig. S6).

Fe and As speciation in the rhizosphere and detritusphere

Arsenic and iron enriched in the root Fe plaques, with their content being approximately threefold higher than that in other samples (Supplementary Fig. S8a, b) ($p < 0.05$). In the Fe plaques, Fe/Al associated As was 10.22 mg/kg, which is approximately tenfold higher than other samples (Supplementary Fig. S8c). The proportions of As

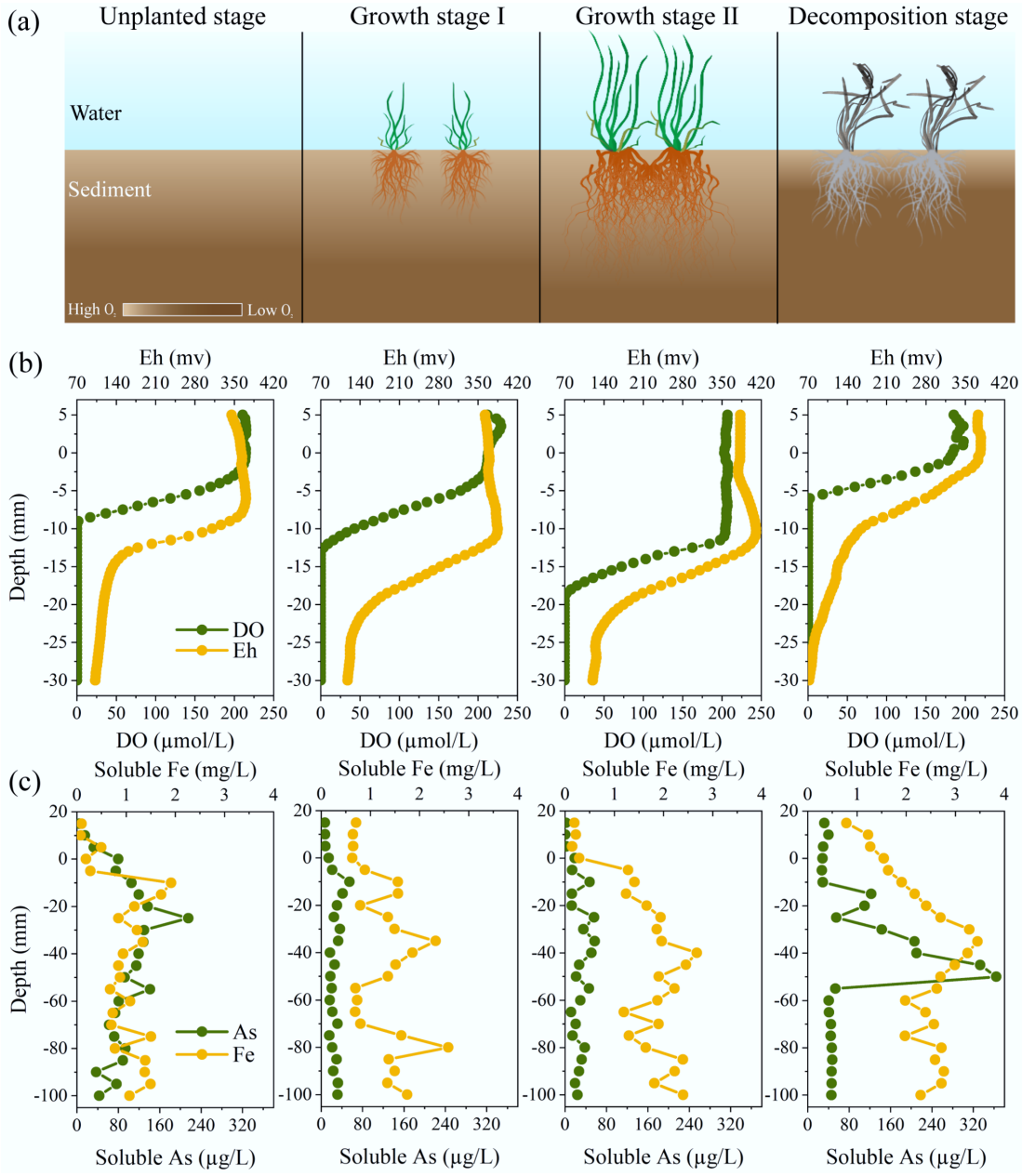

Fig. 1 Changes in physico-chemical properties in sediments during growth and death of submerged macrophytes. **(a)** Schematic illustration of growth and death of macrophytes, which changes the redox environments in sediments. **(b)** Vertical distributions of DO and Eh, and soluble As and Fe in sediments. **(c)** Vertical distributions of soluble As and Fe in sediments.

fractions in the Fe plaques were F_{S1} (0.08%), F_{S2} (0.99%), F_{S3} (17.50%), F_{S4} (3.34%), and F_{S5} (78.09%) (Supplementary Fig. S8d). The F_{S5} was the dominant fraction of As in other samples, and its proportions exceeded 80%. Furthermore, the labile fraction (F_{S1} + F_{S2}) was 1.07% in the Fe plaques, which was lower than that in the rhizosphere (4.89%), detritusphere (5.01%), and bulk sediments (4.43% and 6.60%).

Mössbauer spectra revealed that the (super) paramagnetic Fe(III) fraction (doublet D1) was dominant in both the Fe plaques and rhizosphere, exceeding 76% and 68%, respectively (Fig. 3, Supplementary Table S7). This fraction may include any combination of Fe (oxyhydr) oxides, such as ferrihydrite, lepidocrocite, low-crystalline fractions of hematite, as well as organic-matter-complexed or silicate-associated Fe(III)[42]. Sequential extraction results indicated that the Fe plaques primarily consisted of easily reducible Fe-oxides like ferrihydrite and goethite (Supplementary Fig. S8c). The solid-associated Fe(II) primarily consists of primary minerals, silicate-associated or adsorbed Fe(II) (doublet D2), which exceeded 30% in the detritusphere. D1 fraction was approximately 50% in the detritusphere, lower than that in the Fe plaques and rhizosphere. Additionally, the magnetite fraction increased from the rhizosphere to the detritusphere, surpassing 10%.

Characterization of the microbial community structure and function

PCoA indicated significant differences in microbial communities among the rhizosphere, detritusphere, and bulk sediments (Fig. 4a). No significant differences were found between the bulk sediments of the rhizosphere and detritusphere (p > 0.05), so they were defined

uniformly as bulk sediment for subsequent analyses. The α diversity indexes in the rhizosphere and detritusphere were greater than those in the bulk sediment (Fig. 4b). Proteobacteria were the dominant phylum, with relative abundances ranging from 37.92% to 46.51%, followed by Acidobacteria, Chloroflexi, and Bacteroidetes (Fig. 4c). LEfSe analysis revealed that Proteobacteria and Nitrospirae were significantly enriched in the rhizosphere, while Bacteroidetes, Spirochaetes, and Firmicutes were enriched in the detritusphere (Fig. 4d).

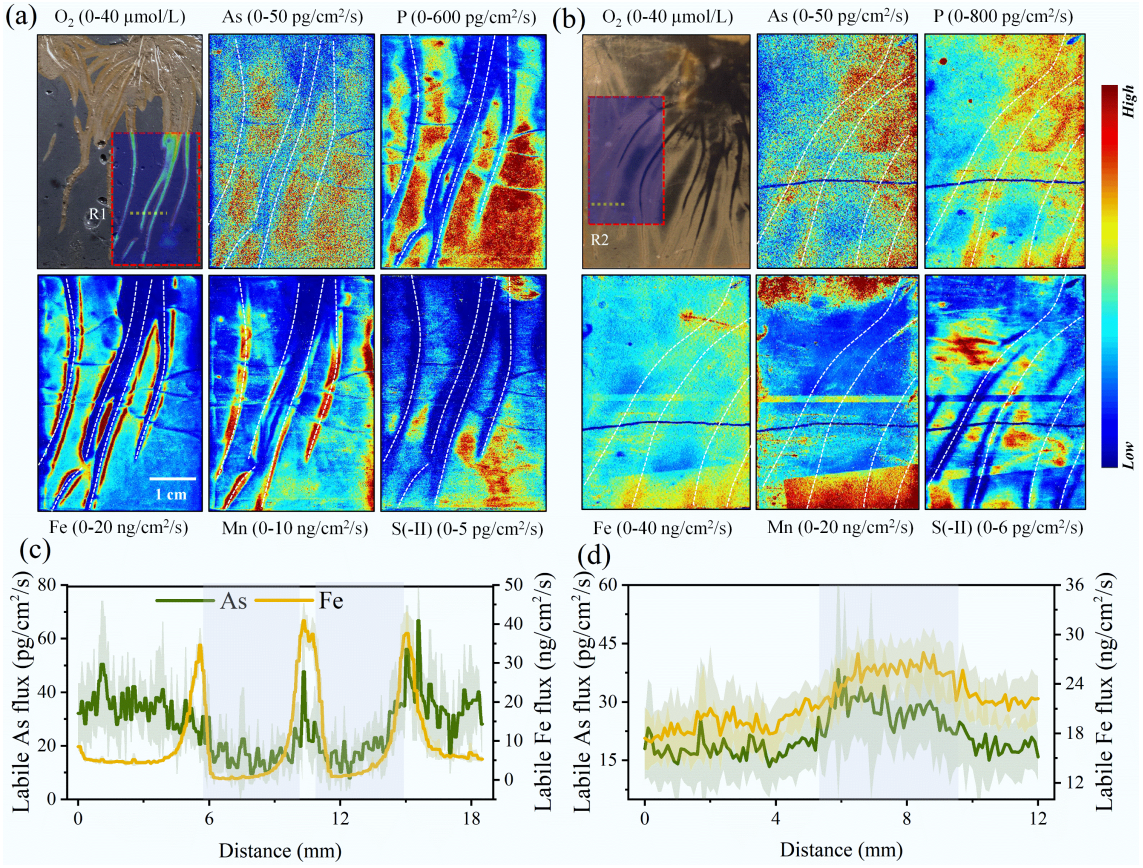

Fig. 2 High-resolution imaging of O_2, As, and other relevant elements in sediments Two-dimensional distribution of O_2 and labile fluxes of As, P, Fe, Mn, and S(-II) in the (**a**) rhizosphere, and (**b**) detritusphere. The white dotted lines represent the position of the roots. One-dimensional distribution of labile fluxes of As and Fe in the (**c**) rhizosphere (R1), and (**d**) detritusphere (R2), grey areas indicate rhizosphere or detritusphere.

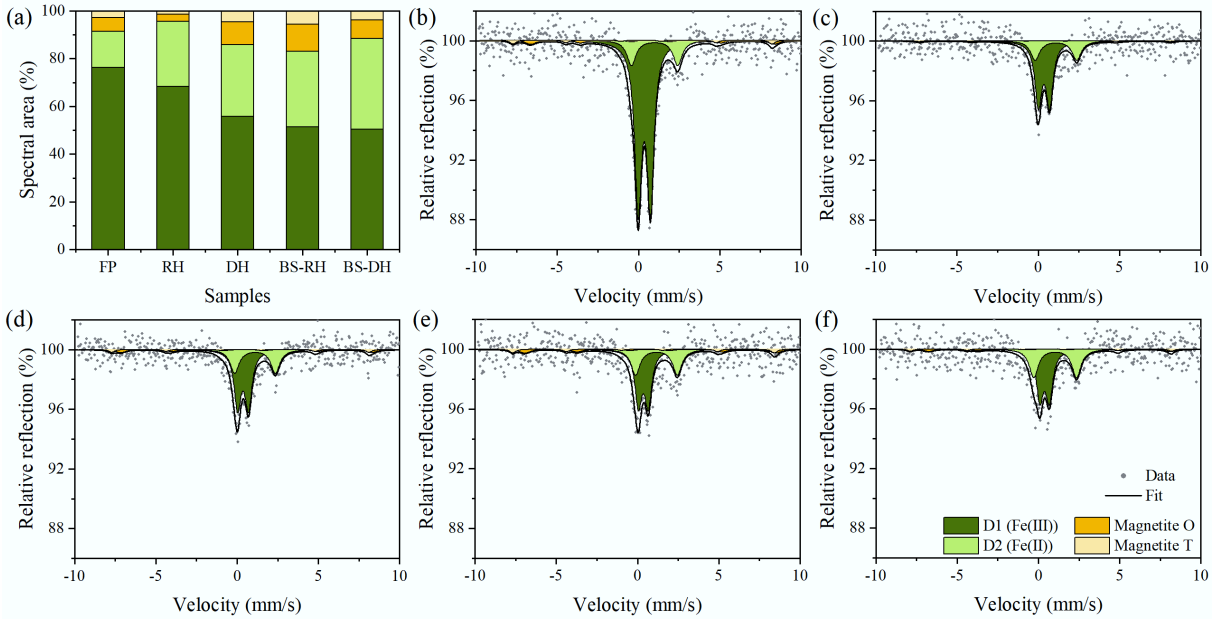

Fig. 3 (**a**) Fe phase fractions, and (**b**) corresponding Mössbauer spectra of Fe plaque (FP), (**c**) rhizosphere (RH), (**d**) detritusphere (DH), (**e**) bulk sediments during macrophytes growth (BS-RH), and (**f**) bulk sediments during macrophytes death (BS-DH).

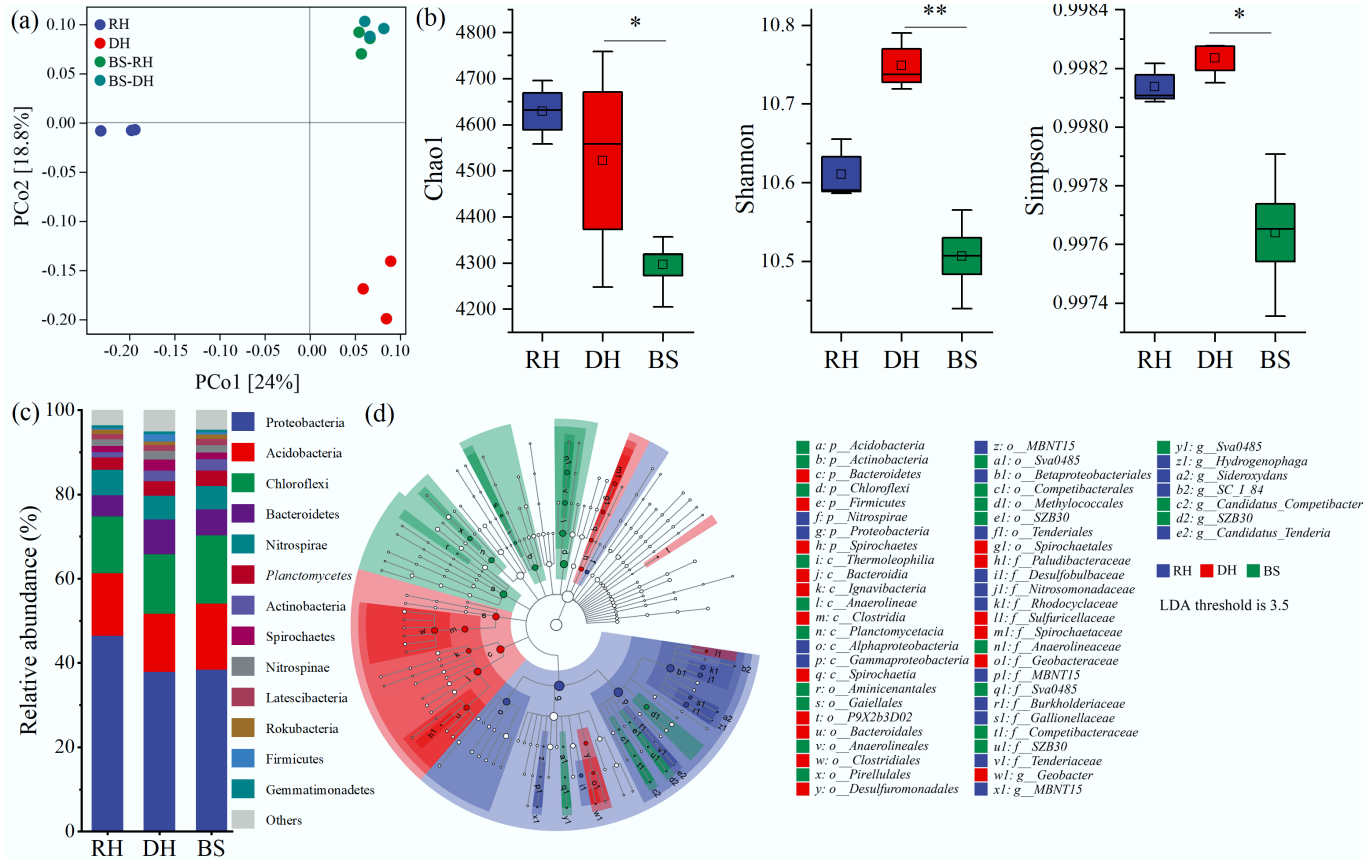

Fig. 4 Microbial diversity and community structures in the rhizosphere (RH), detritusphere (DH), and bulk sediment (BS). (**a**) Composition and structure differences of microbial communities using principal coordinate analysis (PCoA) based on the Bray-Curtis distance, with significant differences analyzed by permutational multivariate analysis of variance (PERMANOVA). (**b**) α-diversity, including the Chao1, Shannon, and Simpson indexes. (**c**) Relative abundance of bacterial communities at the phylum level. (**d**) Bacterial relationships among taxonomic units of microbiota, ranging from the phylum level down to the genus level. Significant differences at * $p < 0.05$, and ** $p < 0.01$.

The bacterial functional profiles related to Fe cycling were characterized using the FAPROTAX tool (Fig. 5a, b). In the rhizosphere, microbes involved in Fe oxidation were more abundant than in the detritusphere and bulk sediment ($p < 0.05$). *Thiobacillus* and *Siderooxydans* were the predominant genera of Fe-oxidizing bacteria in the rhizosphere (Fig. 5c). Conversely, the iron_respiration function was stronger in the detritusphere than in the rhizosphere ($p < 0.05$), with *Geobacter* and *Anaeromyxobacter* being the most dominant Fe-reducing bacterial genus.

The abundances of *ars*M, *aio*A, *arr*A, and *ars*C were 2.76 ± 0.71, 1.15 ± 0.33, 0.02 ± 0.005, and 0.001 ± 0.0004 × 10^6 copies/g in the rhizosphere, respectively, all notably higher than in the detritusphere and bulk sediment ($p < 0.05$) (Fig. 5d–f). They were 4.54, 7.13, 3.36, and 4.17 times lower in the detritusphere than in the rhizosphere for *ars*M, *aio*A, *arr*A, and *ars*C, respectively. There were no significant differences in microbial As-cycling genes between the detritusphere and the bulk sediment ($p > 0.05$). Microbially driven As transformation processes underwent significant changes during the transition from rhizosphere to detritusphere.

Discussion

Decrease in As mobility from bulk sediment to the rhizosphere

The microcosm experiment demonstrated that macrophytes act as a crucial role in remediating sediment As pollution and controlling its release (Fig. 1). A significant negative correlation was observed between the release flux of soluble As and both the O_2 penetration depth and Eh in sediments ($p < 0.01$) (Supplementary Fig. S4), indicating that ROL enhances the oxidative environment in sediments, which is a key factor in reducing As release. High-resolution chemical imaging further supported this finding, revealing lower labile As levels in the aerobic rhizosphere (Fig. 2). The results are consistent with recent studies emphasizing the significant influence of the rhizospheric effects of macrophytes on sediment As remediation[9].

In the aerobic rhizosphere, both the bacterial function involved in Fe oxidation and the abundance of Fe-oxidizing bacteria significantly increased (Fig. 5a, c), promoting Fe(II) oxidation and the development of Fe plaques (Supplementary Fig. S9). Iron plaques are a well-known strong adsorbent for both As(III) and As(V)[43]. Both significant positive correlations between labile Fe and As in both the sediment and rhizosphere ($p < 0.01$) (Supplementary Fig. S10a) suggested that sequestration of Fe plaques is a primary factor contributing to the decrease in As bioavailability. Mössbauer spectra and sequential extraction results showed that Fe plaques were predominantly composed of ferrihydrite and lepidocrocite (Fig. 3 and Supplementary Fig. S8c), consistent with other studies of root plaques in rice observed by EXAFS (X-ray absorption fine structure) spectroscopy[11]. The poorly crystalline Fe minerals may be attributed to ROL-induced rapid redox turnover in the rhizosphere[9]. These Fe minerals are known to exhibit a strong affinity for As[44]. Approximately 20% of As was associated with these Fe minerals in

Fe plaques (Supplementary Fig. S8d), which further supports the role of Fe plaque in immobilizing As. In addition, Fe plaques also have strong adsorption affinities for P[45], which contributes to the decrease in labile P in the rhizosphere (Fig. 2 and Supplementary Fig. S6).

Microorganisms are also critical for altering the As morphology, mobility, and toxicity[46]. Root growth significantly increased the abundance of genes linked to microbe-mediated As cycling in the rhizosphere ($p < 0.05$) (Fig. 5d–f). Microbially mediated As(III) methylation and oxidation can transform As(III), which has stronger mobility and toxicity, into organic As with lower toxicity, and As(V) with lower mobility, respectively[47]. Therefore, root-regulated improvement in microbial As(III) methylation and oxidation is another important reason for the reduction in sediment As immobilization. Genes involved in both respiratory As(V) reduction (*arr*A), and detoxifying As(V) reduction (*ars*C) showed a greater abundance in the rhizosphere compared to bulk sediments. In the rhizosphere, As(V) is the dominant As species, which provides sufficient reaction substrates for microbial reduction[46]. Although the rhizosphere showed a greater abundance of genes related to As reduction compared to bulk sediments, this was considerably lower than the abundance of As(III) methylation and oxidation genes.

Interestingly, labile Fe increased sharply at the boundary between the rhizosphere and bulk sediment (Fig. 2 and Supplementary Fig. S6). Root-induced formation of an aerobic–anaerobic interface may create a niche for Fe(III)-reducing bacteria, facilitating the reduction of Fe minerals[48,49]. This process might facilitate biogeochemical cycles of pollutants at the rhizosphere–sediment interface, which warrants further exploration. Labile Mn exhibited an opposite trend compared to labile Fe in the rhizosphere, showing significant negative correlations with labile P and As (Fig. 2, Supplementary Figs S6 and S10a). Carboxylates secreted from roots occur to mobilize the low-availability P, which might coincidentally enhance Mn availability in the rhizosphere[50]. Additionally, studies have indicated that Mn-oxides in the rhizosphere can chemically oxidate As(III) to As(V)[9,51]. The above processes not only promote rapid oxidation of As(III) and subsequent sorption of As(V) to Fe plaques, but also increase the Mn solubilization in the rhizosphere.

Increase in As mobility from the rhizosphere to the detritusphere

As the rhizosphere transitions to the detritusphere, changes take place such as to the microbial community structure[17,52]. However, it is still unknown whether the legacy effects of roots have implications for the mobility of As. We first found that root decomposition of macrophytes can enhance the release of As from sediments and raise the risk of aqueous As contamination. After the death of *V. natans*, the soluble As and labile As in sediments increased approximately 3.5-fold and 2-fold, respectively, compared to their levels during plant growth (Figs 1 and 2). An increase in the concentration gradient at the sediment-water surface further promoted the diffusive transport of As from sediment to overlying water (Supplementary Fig. S4).

The release of O_2 from roots ceased after plants wither, coupled with the consumption of O_2 by root degradation, transforming the aerobic rhizosphere into an anaerobic detritusphere (Fig. 2 and Supplementary Fig. S3). In O_2-limited sediment, reductive dissolution of easily reducible Fe-oxides by Fe-reducing microorganisms is favored[53]. Previous studies have discovered that when Fe plaques are exposed to Fe(III)-reducing bacteria, approximately 30% of Fe(II) is remobilized, and more than 50% is converted by microbes to Fe(II) minerals[54]. This is consistent with our observations of Mössbauer spectra, which show a decrease in the (super)paramagnetic Fe(III) fraction, with an increase in the solid-associated Fe(II) fraction in the

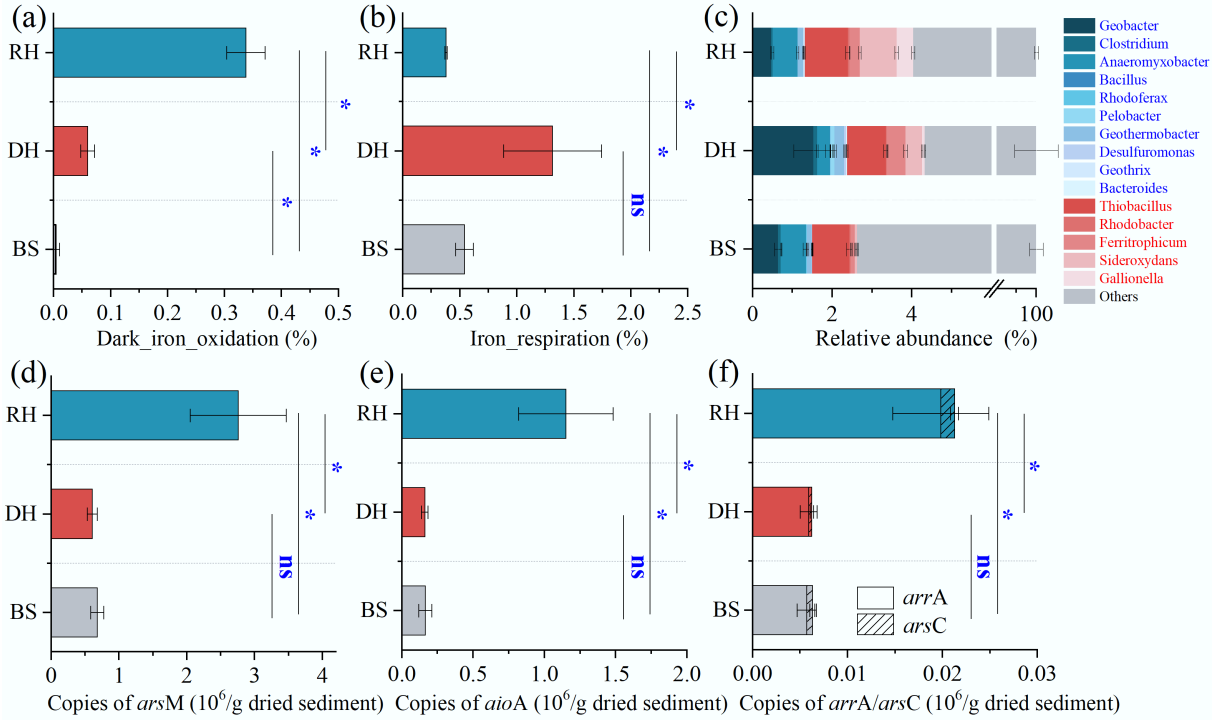

Fig. 5 Relative 16S rRNA (gene) abundance of Fe-cycling microbial communities and absolute quantification of As biotransformation genes in the rhizosphere (RH), detritusphere (DH), and bulk sediment (BS). (**a**) Dark_iron_oxidation function. (**b**) Iron_respiration function. (**c**) Relative abundance of typical Fe-reducing (bule text), and Fe-oxidizing (red text) bacteria. (**d**)–(**f**) Abundance of the *ars*M, *aio*A, *arr*A, and *ars*C, respectively. Significance levels at * $p < 0.05$; ns, not significant.

detritusphere compared to Fe plaque and rhizosphere (Fig. 3). The iron_respiration function significantly increased from the rhizosphere to the detritusphere, especially the Fe-reducing bacteria *Geobacter* (Figs. 4b, c), which plays a crucial role in reductive dissolution of Fe(III) minerals in Fe plaques.

After the death of *V. natans*, Fe(III) minerals formed during root growth may undergo rapid reduction; indeed, few root Fe deposits were collected from the detritusphere in this study (Fig. 2). This result suggests a significant reduction in the ability of the natural reactive barrier (Fe[III] minerals) to trap As in the detritusphere. In this study, there was 79.38% of total As lost from the Fe plaque (Supplementary Fig. S8b), which was comparable to the loss value measured in rice root Fe plaque i.e., 76.1% of total As loss within 27 d of degradation[20]. According to As fraction analysis, approximately 90% of Fe-bound As is lost during this process (Supplementary Fig. S8d). In the detritusphere, there was a significant positive correlation between labile As and Fe ($p < 0.01$) (Supplementary Fig. S10b), further demonstrating that reductive dissolution of Fe plaques is an important reason for the release of As from the sediment.

In the detritusphere, significant changes in As metabolism genes were observed when compared to the rhizosphere ($p < 0.05$) (Fig. 5d–f). Particularly, genes involved in As methylation, oxidation, and reduction exhibited a marked decline from the rhizosphere to the detritusphere, while they showed no significant differences between the detritusphere and bulk sediment. During macrophyte growth, roots create niches for microbial communities involved in As cycling, especially those microbes mediating As methylation and oxidation[9,55]. However, after the death of macrophytes, as the rhizosphere transitions to the detritusphere, the release of exudates and oxygen ceases, causing the collapse of specific rhizospheric microniches. This disrupts the microbial processes of As(III) oxidation and methylation driven by root growth. As a result, the decline in these microbe-driven processes contributes to an increase in As mobility and bioavailability in the sediment.

Implications on aqueous As contamination

Two microcosm experiments were performed to reveal an overlooked pathway of aqueous As contamination, whereby sediment shifts from a sink to a source of As after macrophyte death. In the rhizosphere, the microbe-driven As(III) methylation and oxidation, along with Fe plaque sequestration, reduce the toxicity and mobility of As, resulting in a downward movement of soluble As from the overlying water into the sediment (Fig. 6). Recent studies suggest that submerged macrophytes have decreased by 30.4% in global lakes over the past two decades[16,56], and therefore the ability of the rhizosphere to alleviate sediment As pollution may vary in response to the transition from rhizosphere to detritusphere. After the death of macrophytes, the rhizosphere switches from controlling the mobility of As in sediments to functioning as the release hotspots of As driven by microbial decomposition of Fe plaques and reduced As biotransformation in the detritusphere (Fig. 6). Considering the widespread occurrence of macrophyte loss, it is possible that the 'rhizosphere traps' unexpectedly serve as a source of As, potentially exacerbating As pollution in waterbodies. Moreover, localized increases of labile P and S(-II) in the detritusphere may further threaten water quality.

Our findings also offer valuable insights for water ecological restoration that not only focus on removing contaminations via macrophytes, but also consider the long-term impacts of their loss or seasonal death on sediment nature and water quality. Effective lake and waterbody management should integrate these potential processes into sediment and aquatic plant restoration strategies. By recognizing the dual role of 'rhizosphere traps' as both sinks and sources of contamination, we can develop effective measures ensuring the potential risks posed by macrophyte loss or seasonal death. For example, capping materials with oxidative functions can be applied to the sediment surface or mixed into the upper sediment layer[57,58], which specifically target As immobilization under the reducing conditions that develop in the detritusphere. This study offers new perspectives on how the growth and decomposition of macrophyte roots affect the mobilization of As in sediments. This knowledge can help us recognize and assess potential threats to

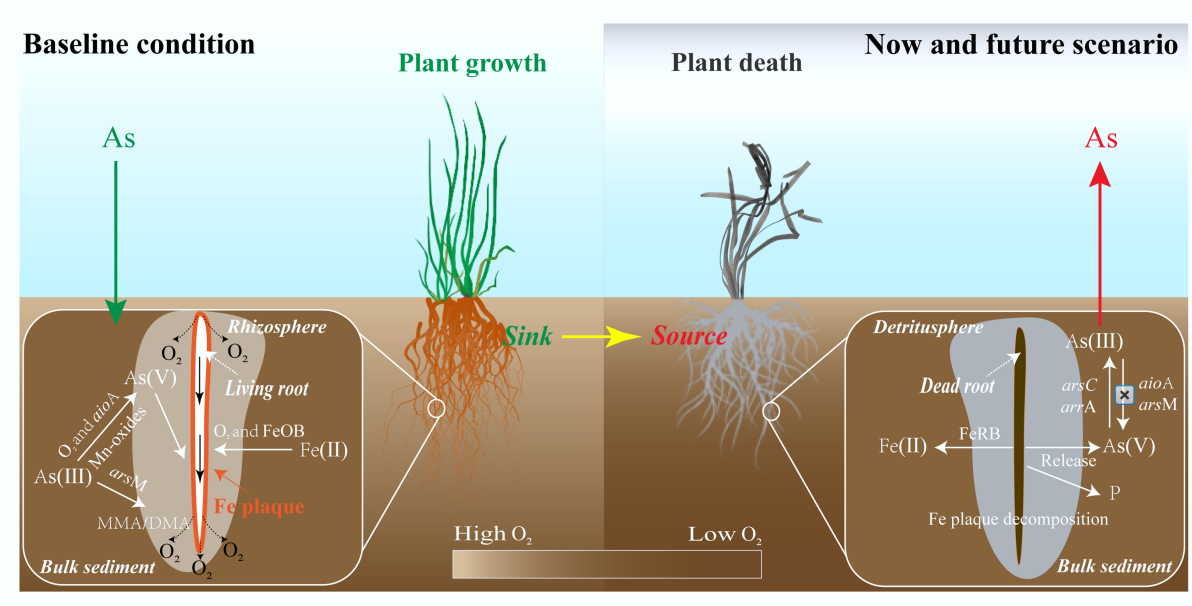

Fig. 6 Conceptual diagram of As mobilization processes in the rhizosphere and detritusphere. Baseline conditions (left) are compared to now and future scenarios (right) of widespread loss of submerged macrophytes.

water quality and ecosystems, particularly the possible release of pollutants enriched in the rhizosphere.

Conclusions

The findings of this study suggest that sediment shifts from a sink to a source of As after macrophyte death, as a result of differences in abiotic and biotic transformation of Fe and As between rhizosphere and detritusphere. During root growth, microbe-driven As(III) methylation and oxidation, as well as Fe plaque sequestration, increased the As immobilization in the rhizosphere. However, following macrophyte death, the combined effects of Fe plaque dissolution and impaired microbial-mediated As transformation significantly increased As mobilization, resulting in a net flux of As into the overlying water from sediments. It is important to note that future work should incorporate pH and organic matter dynamics, as root decomposition alters these factors, potentially affecting As mobility via competitive adsorption and complexation. This study offers new perspectives on how the growth and decomposition of macrophyte roots affect the mobilization of As in sediments, which can serve as a warning sign of aqueous As contamination, especially considering the widespread loss of submerged macrophytes globally.

Supplementary information

It accompanies this article at: https://doi.org/10.48130/een-0025-0003.

Author contributions

All authors contributed to the study conception and design. Material preparation, data collection, and analysis were performed by Cai Li, Xin Ma, Xue Jiang, and Youzi Gong. The first draft of the manuscript was written by Cai Li. Xiaolong Wang, Musong Chen, Qin Sun, and Shiming Ding discussed the results and commented on the manuscript. All authors reviewed the results and approved the final version of the manuscript.

Data availability

The datasets used or analyzed during the current study are available from the corresponding author upon reasonable requests.

Acknowledgments

We thank Zhilin Zhong for assistance with macrophyte cultivation and Mingyi Ren for assistance with instrumental methods of analysis.

Funding

This study was funded by the National Natural Science Foundation of China (U2102210, 42407535, and 42277393), the China Postdoctoral Science Foundation (GZB20230782, 2024M763366), the Basic Research Program of Jiangsu (BK20241697), the Key Research and Development Program of Jiangxi Province (20223BBG74003), and the Long-term Program for Innovative Leading Talents of Jiangxi Province (jxsq2023101034).

Declarations

Competing interests

The authors declare that they have no conflict of interest.

Author details

[1]State Key Laboratory of Lake and Watershed Science for Water Security, Nanjing Institute of Geography and Limnology, Chinese Academy of Sciences, Nanjing 211135, China; [2]School of Hydrology and Water Resources, Hohai University, Nanjing 210098, China; [3]School of Chemical Science and Technology, Yunnan University, Kunming 650091, China; [4]Key Laboratory of Integrated Regulation and Resource Development on Shallow Lakes, Ministry of Education, College of Environment, Hohai University, Nanjing 210098, China; [5]School of Energy and Environment, Southeast University, Nanjing 211189, China

References

[1] Bowell RJ, Alpers CN, Jamieson HE, Nordstrom DK, Majzlan J. 2014. The environmental geochemistry of arsenic - an overview. *Reviews in Mineralogy and Geochemistry* 79:1–16

[2] Mukherjee A, Coomar P, Sarkar S, Johannesson KH, Fryar AE, et al. 2024. Arsenic and other geogenic contaminants in global groundwater. *Nature Reviews Earth & Environment* 5:312–28

[3] Osuna-Martínez CC, Armienta MA, Bergés-Tiznado ME, Páez-Osuna F. 2021. Arsenic in waters, soils, sediments, and biota from Mexico: An environmental review. *Science of the Total Environment* 752:142062

[4] Duan L, Song J, Yin M, Liu X, Liu X, et al. 2024. Hypoxia exacerbate the marine ecological risk of arsenic: By stimulating its migration and release at the sediment-water interface. *Water Research* 268:122603

[5] Luo T, Sun Y, Liang W, Zheng Q, Kong S, et al. 2025. The alternation of flood and ebb tide induced arsenic release and migration from coastal tidal flat sediments in Yellow Sea wetlands: an ex-situ study. *Journal of Cleaner Production* 448:141730

[6] Wallis I, Prommer H, Berg M, Siade AJ, Sun J, et al. 2020. The river–groundwater interface as a hotspot for arsenic release. *Nature Geoscience* 13:288–295

[7] Barrett PM, Hull EA, Burkart K, Hargrave O, McLean J, et al. 2019. Contrasting arsenic cycling in strongly and weakly stratified contaminated lakes: Evidence for temperature control on sediment–water arsenic fluxes. *Limnology and Oceanography* 64:1333–1346

[8] Fan Y, Sun S, He S. 2023. Iron plaque formation and its effect on key elements cycling in constructed wetlands: Functions and outlooks. *Water Research* 235:119837

[9] Li C, Ding S, Ma X, Wang Y, Sun Q, et al. 2023. Sediment arsenic remediation by submerged macrophytes via root-released O_2 and microbe-mediated arsenic biotransformation. *Journal of Hazardous materials* 449:131006

[10] Maisch M, Lueder U, Kappler A, Schmidt C. 2019. Iron lung: how rice roots induce iron redox changes in the rhizosphere and create niches for microaerophilic Fe(II)-oxidizing bacteria. *Environmental Science & Technology Letters* 6:600–605

[11] Limmer MA, Evans AE, Seyfferth AL. 2021. A new method to capture the spatial and temporal heterogeneity of aquatic plant iron root plaque *in situ*. *Environmental Science & Technology* 55:912–918

[12] Fresno T, Peñalosa JM, Santner J, Puschenreiter M, Prohaska T, et al. 2016. Iron plaque formed under aerobic conditions efficiently immobilizes arsenic in Lupinus albus L roots. *Environmental Pollution* 216:215–222

[13] Meng FL, Zhang X, Hu Y, Sheng GP. 2024. New barrier role of iron plaque: producing interfacial hydroxyl radicals to degrade rhizosphere pollutants. *Environmental Science & Technology* 58:795–804

[14] Zhang SY, Zhao FJ, Sun GX, Su JQ, Yang XR, et al. 2015. Diversity and abundance of arsenic biotransformation genes in paddy soils from Southern China. *Environmental Science & Technology* 49:4138–4146

[15] Phillips G, Willby N, Moss B. 2016. Submerged macrophyte decline in shallow lakes: What have we learnt in the last forty years? *Aquatic Botany* 135:37–45

[16] Luo J, Duan H, Xu Y, Shen M, Zhang Y, et al. 2025. Global trends and regime state shifts of lacustrine aquatic vegetation. *The Innovation* 6:100784

[17] Mueller CW, Baumert V, Carminati A, Germon A, Holz M, et al. 2024. From rhizosphere to detritusphere – Soil structure formation driven by plant roots and the interactions with soil biota. *Soil Biology and Biochemistry* 193:109396

[18] Fang W, Williams PN, Zhang H, Yang Y, Yin D, et al. 2021. Combining multiple high-resolution *in situ* techniques to understand phosphorous availability around rice roots. *Environmental Science & Technology* 55:13082–13092

[19] Kappler A, Bryce C, Mansor M, Lueder U, Byrne JM, et al. 2021. An evolving view on biogeochemical cycling of iron. *Nature Reviews Microbiology* 19:360–374

[20] Huang H, Zhu Y, Chen Z, Yin X, Sun G. 2012. Arsenic mobilization and speciation during iron plaque decomposition in a paddy soil. *Journal of Soils and Sediments* 12:402–410

[21] Witzgall K, Steiner FA, Hesse BD, Riveras-Muñoz N, Rodríguez V, et al. 2024. Living and decaying roots as regulators of soil aggregation and organic matter formation—from the rhizosphere to the detritusphere. *Soil Biology and Biochemistry* 197:109503

[22] Zhang Y, Jeppesen E, Liu X, Qin B, Shi K, et al. 2017. Global loss of aquatic vegetation in lakes. *Earth-Science Reviews* 173:259–265

[23] Kuzyakov Y, Razavi BS. 2019. Rhizosphere size and shape: Temporal dynamics and spatial stationarity. *Soil Biology and Biochemistry* 135:343–360

[24] Lippold E, Schlüter S, Mueller CW, Höschen C, Harrington G, et al. 2023. Correlative imaging of the rhizosphere horizontal line: a multimethod workflow for targeted mapping of chemical gradients. *Environmental Science & Technology* 57:1538–1549

[25] Cui J, Wang Y, Ding S, Chen M, Li D, et al. 2024. High-resolution diurnal variation mechanism of oxygen and acid environments at the water–sediment interface during cyanobacterial decomposition. *Journal of Cleaner Production* 435:140605

[26] Tang N, Huang W, Li X, Gao X, Liu X, et al. 2024. Drilling into the physiology, transcriptomics, and metabolomics to enhance insight on Vallisneria denseserrulata responses to nanoplastics and metalloid co-stress. *Journal of Cleaner Production* 448:141730

[27] Zhang Q, Dong X, Yang X, Liu E, Lin Q, et al. 2022. Aquatic macrophyte fluctuations since the 1900s in the third largest Chinese freshwater lake (Lake Taihu): evidences, drivers and management implications. *CATENA* 213:106153

[28] Li C, Ding S, Yang L, Wang Y, Ren M, et al. 2019. Diffusive gradients in thin films: devices, materials and applications. *Environmental Chemistry Letters* 17:801–31

[29] Ma X, Song Y, Shen Y, Yang L, Ding S, et al. 2024. Fine-scale measurements unravel the side effects of biochar capping on the bioavailability and mobility of phosphorus in sediments. *Biochar* 6:49

[30] Li C, Ding S, Yang L, Zhu Q, Chen M, et al. 2019. Planar optode: a two-dimensional imaging technique for studying spatial-temporal dynamics of solutes in sediment and soil. *Earth-Science Reviews* 197:102916

[31] Li C, Ding S, Chen M, Zhong Z, Sun Q, et al. 2023. Visualizing biogeochemical heterogeneity in soils and sediments: a review of advanced micro-scale sampling and imaging methods. *Critical Reviews in Environmental Science and Technology* 53:1229–1253

[32] Guan DX, He SX, Li G, Teng HH, Ma LQ. 2022. Application of diffusive gradients in thin-films technique for speciation, bioavailability, modeling and mapping of nutrients and contaminants in soils. *Critical Reviews in Environmental Science and Technology* 52:3035–3079

[33] Ren M, Ding S, Dai Z, Wang J, Li C, et al. 2021. A new DGT technique comprising a hybrid sensor for the simultaneous high resolution 2-D imaging of sulfides, metallic cations, oxyanions and dissolved oxygen. *Journal of Hazardous Materials* 403:123597

[34] Smolders E, Wagner S, Prohaska T, Irrgeher J, Santner J. 2020. Sub-millimeter distribution of labile trace element fluxes in the rhizosphere explains differential effects of soil liming on cadmium and zinc uptake in maize. *Science of the Total Environment* 738:140311

[35] Notini L, Schulz K, Kubeneck LJ, Grigg ARC, Rothwell KA, et al. 2023. A new approach for investigating iron mineral transformations in soils and sediments using ^{57}Fe-labeled minerals and ^{57}Fe Mössbauer spectroscopy. *Environmental Science & Technology* 57:10008–10018

[36] Wang D, Zhu MX, Yang GP, Ma WW. 2019. Reactive iron and iron-bound organic carbon in surface sediments of the river-dominated Bohai Sea (China) versus the Southern Yellow Sea. *Journal of Geophysical Research: Biogeosciences* 124:79–98

[37] Wan X, Dong H, Feng L, Lin Z, Luo Q. 2017. Comparison of three sequential extraction procedures for arsenic fractionation in highly polluted sites. *Chemosphere* 178:402–410

[38] Wang S, Ding S, Zhao H, Chen M, Yang D, et al. 2024. Seasonal variations in spatial distribution, mobilization kinetic and toxicity risk of arsenic in sediments of Lake Taihu, China. *Journal of Hazardous Materials* 463:132852

[39] Larsen M, Santner J, Oburger E, Wenzel WW, Glud RN. 2015. O_2 dynamics in the rhizosphere of young rice plants (*Oryza sativa* L. *) as studied by planar optodes. Plant and Soil* 390:279–292

[40] Santner J, Larsen M, Kreuzeder A, Glud RN. 2015. Two decades of chemical imaging of solutes in sediments and soils – a review. *Analytica Chimica Acta* 878:9–42

[41] Han C, Ren J, Tang H, Xu D, Xie X. 2016. Quantitative imaging of radial oxygen loss from *Valisneria spiralis* roots with a fluorescent planar optode. *Science of the Total Environment* 569–570:1232–1240

[42] Schulz K, Wisawapipat W, Barmettler K, Grigg ARC, Kubeneck LJ, et al. 2024. Iron Oxyhydroxide Transformation in a Flooded Rice Paddy Field and the Effect of Adsorbed Phosphate. *Environmental Science & Technology* 58:10601–10610

[43] Yamaguchi N, Ohkura T, Takahashi Y, Maejima Y, Arao T. 2014. Arsenic distribution and speciation near rice roots influenced by iron plaques and redox conditions of the soil matrix. *Environmental Science & Technology* 48:1549–1556

[44] Meng D, Nabi F, Kama R, Li S, Wang W, et al. 2024. The interaction between ferrihydrite and arsenic: a review of environmental behavior, mechanism and applied in remediation. *Journal of Hazardous Materials Advances* 13:100398

[45] Xing X, Ding S, Liu L, Chen M, Yan W, et al. 2018. Direct evidence for the enhanced acquisition of phosphorus in the rhizosphere of aquatic plants: a case study on *Vallisneria natans*. *Science of the Total Environment* 616–617:386–396

[46] Zhou M, Liu Z, Zhang B, Yang J, Hu B. 2022. Interaction between arsenic metabolism genes and arsenic leads to a lose-lose situation. *Environmental Pollution* 312:119971

[47] Zhu YG, Xue XM, Kappler A, Rosen BP, Meharg AA. 2017. Linking genes to microbial biogeochemical cycling: lessons from arsenic. *Environmental Science & Technology* 51:7326–7339

[48] Zhong Z, Li C, Chen M, Zhao H, Fan X, et al. 2023. The root tip of submerged plants: an efficient engine for carbon mineralization. *Environmental Science and Technology Letters* 10:385–390

[49] Yao J, Qin S, Liu T, Clough TJ, Wrage-Mönnig N, et al. 2022. Rice root Fe plaque enhances oxidation of microbially available organic carbon via Fe(III) reduction-coupled microbial respiration. *Soil Biology and Biochemistry* 167:108568

[50] Lambers H, Hayes PE, Laliberté E, Oliveira RS, Turner BL. 2015. Leaf manganese accumulation and phosphorus-acquisition efficiency. *Trends in Plant Science* 20:83–90

[51] Wagner S, Hoefer C, Puschenreiter M, Wenzel WW, Oburger E, et al. 2020. Arsenic redox transformations and cycling in the rhizosphere of Pteris vittata and Pteris quadriaurita. *Environmental and Experimental Botany* 177:104122

[52] Teixeira PPC, Vidal A, Teixeira APM, Souza IF, Hurtarte LCC, et al. 2024. Decoding the rhizodeposit-derived carbon's journey into soil organic matter. *Geoderma* 443:116811

[53] Patzner MS, Logan M, McKenna AM, Young RB, Zhou Z, et al. 2022. Microbial iron cycling during palsa hillslope collapse promotes greenhouse gas emissions before complete permafrost thaw. *Communications Earth & Environment* 3:76

[54] Maisch M, Lueder U, Kappler A, Schmidt C. 2020. From plant to paddy—how rice root iron plaque can affect the paddy field iron cycling. *Soil Systems* 4:28

[55] Qiao J, Liu J, Palomo A, Bostick BC, Phan K, et al. 2023. Prevalence of methylated arsenic and microbial arsenic methylation genes in paddy soils of the Mekong Delta. *Environmental Science & Technology* 57:9675–9682

[56] Yu H, Lu Q, Cao X, Wang Y, Xu Y, et al. 2024. Habitat disturbance drives the feedback of aquatic plants on the microbial community after lake degradation. *ACS ES&T Water* 4:3509–3520

[57] Tang Y, Zhang M, Zhang J, Lyu T, Cooper M, et al. 2021. Reducing arsenic toxicity using the interfacial oxygen nanobubble technology for sediment remediation. *Water Research* 205:117657

[58] Jiang X, Gong Y, Xiong J, Ren B, Qiu Y, et al. 2025. Reducing arsenic mobilization in sediments: a synergistic effect of oxidation and adsorption with zirconium-manganese binary metal oxides. *Water Research* 283:123798